

Phonon transport properties of Janus Pb_2XAs (X = P, Sb, and Bi) monolayers: A DFT study

Jiaxin Geng(耿嘉鑫), Pei Zhang(张培), Zhunyun Tang(汤准韵), and Tao Ouyang(欧阳滔)

Citation: Chin. Phys. B, 2024, 33 (**4**): 046501. DOI: 10.1088/1674-1056/ad2260
Journal homepage: http://cpb.iphy.ac.cn; http://iopscience.iop.org/cpb

What follows is a list of articles you may be interested in

Lattice thermal conductivity switching via structural phase transition in ferromagnetic VI_3

Chao Wu(吴超) and Chenhan Liu(刘晨晗)
Chin. Phys. B, 2023, 32 (**5**): 056502. DOI: 10.1088/1674-1056/acb764

Effects of phonon bandgap on phonon-phonon scattering in ultrahigh thermal conductivity ϑ-phase TaN

Chao Wu(吴超) and Chenhan Liu(刘晨晗)
Chin. Phys. B, 2023, 32 (**4**): 046502. DOI: 10.1088/1674-1056/acb201

Near-zero thermal expansion in β-$CuZnV_2O_7$ in a large temperature range

Yaguang Hao(郝亚光), Hengli Xie(谢恒立), Gaojie Zeng(曾高杰), Huanli Yuan(袁焕丽), Yangming Hu(胡杨明), Juan Guo(郭娟), Qilong Gao(高其龙), Mingju Chao(晁明举), Xiao Ren(任霄), and Er-Jun Liang(梁二军)
Chin. Phys. B, 2022, 31 (**4**): 046502. DOI: 10.1088/1674-1056/ac3393

Lattice thermal conductivity of β_{12} and χ_3 borophene

Jia He(何佳), Yulou Ouyang(欧阳宇楼), Cuiqian Yu(俞崔前), Pengfei Jiang(蒋鹏飞), Weijun Ren(任卫君), and Jie Chen(陈杰)
Chin. Phys. B, 2020, 29 (**12**): 126503. DOI: 10.1088/1674-1056/abbbe6

Low lattice thermal conductivity and high figure of merit in p-type doped K_3IO

Weiqiang Wang(王巍强), Zhenhong Dai(戴振宏), Qi Zhong(钟琦), Yinchang Zhao(赵银昌), and Sheng Meng(孟胜)
Chin. Phys. B, 2020, 29 (**12**): 126501. DOI: 10.1088/1674-1056/abab83

SPECIAL TOPIC — Heat conduction and its related interdisciplinary areas

Phonon transport properties of Janus Pb_2XAs (X = P, Sb, and Bi) monolayers: A DFT study

Jiaxin Geng(耿嘉鑫)[1,†], Pei Zhang(张培)[2,†], Zhunyun Tang(汤准韵)[1,‡], and Tao Ouyang(欧阳滔)[1,§]

[1] *School of Physics and Optoelectronics and Hunan Key Laboratory for Micro-Nano Energy Materials and Device, Xiangtan University, Xiangtan* 411105, *China*

[2] *Hunan Provincial Key Laboratory of Intelligent Sensors and Advanced Sensor Materials, School of Physics and Electronics, Hunan University of Science and Technology, Xiangtan* 411201, *China*

(Received 6 December 2023; revised manuscript received 20 January 2024; accepted manuscript online 25 January 2024)

Grasping the underlying mechanisms behind the low lattice thermal conductivity of materials is essential for the efficient design and development of high-performance thermoelectric materials and thermal barrier coating materials. In this paper, we present a first-principles calculations of the phonon transport properties of Janus Pb_2PAs and Pb_2SbAs monolayers. Both materials possess low lattice thermal conductivity, at least two orders of magnitude lower than graphene and h-BN. The room temperature thermal conductivity of Pb_2SbAs (0.91 W/mK) is only a quarter of that of Pb_2PAs (3.88 W/mK). We analyze in depth the bonding, lattice dynamics, and phonon mode level information of these materials. Ultimately, it is determined that the synergistic effect of low group velocity due to weak bonding and strong phonon anharmonicity is the fundamental cause of the intrinsic low thermal conductivity in these Janus structures. Relative regular residual analysis further indicates that the four-phonon processes are limited in Pb_2PAs and Pb_2SbAs, and the three-phonon scattering is sufficient to describe their anharmonicity. In this study, the thermal transport properties of Janus Pb_2PAs and Pb_2SbAs monolayers are illuminated based on fundamental physical mechanisms, and the low lattice thermal conductivity endows them with the potential applications in the field of thermal barriers and thermoelectrics.

Keywords: lattice thermal conductivity, weak bonding, phonon anharmonicity, first principles calculations

PACS: 65.40.–b, 63.20.kg, 63.20.Ry, 63.20.dk **DOI:** 10.1088/1674-1056/ad2260

1. Introduction

Materials with low lattice thermal conductivity (κ_L) have received much attention for their potential applications in thermal barrier coatings,[1,2] thermoelectrics,[3–6] and efficient thermal management. Meanwhile, the thermal transport in semiconductors is mainly controlled by phonon transport, which makes the regulation of lattice thermal conductivity crucial. Up to today, applying external fields (force, electric, magnetic),[7–9] doping,[10] alloying,[11] and constructing superlattices[12] are popular strategies to reduce the κ_L. In addition, finding materials with inherently low κ_L will make regulation more efficient and further contribute to its application in fields such as thermoelectrics. Over the past few decades, considerable progress has been made in understanding the underlying mechanisms of various compounds with low thermal conductivity.[13–17] For example, the low κ_L in ordered crystalline chalcogenides (Cu_3SbSe_4, Cu_3SbSe_3, and $CuSbSe_2$), cage structure (Zn_4Sb_3 and $Eu_8Ga_{16}Ge_{30}$), and lead chalcogenide with rocksalt structure (SnTe, Bi_2Te_3, Bi, and Sb) originates from the strong anharmonicity due to the lone-pair electrons,[14] rattling atoms,[15,16] and resonant bonding,[17] respectively. Since the strong phonon–phonon interactions can produce intrinsically low κ_L while maintaining carrier mobility, the inherent strong anharmonicity of materials also plays a key role in the exploration of high-performance thermoelectric devices.

The study of phonon transport in two-dimensional (2D) materials is one of the hottest topics in materials science and condensed matter physics over the last two decades.[18–23] Unfortunately, certain classical 2D materials, e.g., graphene,[21,23] h-BN,[24,25] and MoS_2[26–28] face significant constraints in their application as thermoelectric materials due to their elevated thermal conductivity. The group IV–V layered material M_2X_2 (M = Si, Ge, Sn, Pb; X = P, As, Sb, Bi) is mainly characterized by two stable configurations with space groups of $C2/m$ and P-6m2 (mostly semiconductor materials).[29–33] Benefiting from the weaker interlayer van der Waals interactions, two-dimensional sheets of Si_2As_2, Ge_2P_2, and Ge_2As_2 with $C2/m$ phases are experimentally prepared.[31–33] Thereafter, it has inspired several theoretical studies about monolayer M_2X_2 ($C2/m$).[34–37] However, in recent years, there appears to be a heightened research focuses on the monolayer P-6m2 phase M_2X_2, primarily due to its appealing optical, thermoelectric, and distinctive Mexican-hat-shaped electronic energy band properties.[30,38–41] Moreover,

[†]These authors contributed equally to this work.

[‡]Corresponding author. E-mail: 202331520177@smail.xtu.edu.cn

[§]Corresponding author. E-mail: ouyangtao@xtu.edu.cn

© 2024 Chinese Physical Society and IOP Publishing Ltd

more interesting behaviors are found in this Janus structure where the mirror symmetry is broken. For example, Wu *et al*. demonstrated the remarkable piezoelectric properties of monolayers of Janus X_2PAs (X = Si, Ge, and Sn).[42] He and Liu *et al*. concluded that Janus X_2PAs possesses superior photocatalytic performance with high carrier mobility.[43,44] Liu and Touski *et al*. found an interesting Rashba effect and Lifshitz transition in Janus PA_2As (A = Si, Ge, Sn, and Pb), XSn$_2Y$, and Si$_2XY$ (X,Y = P, As, Sb, and Bi; $X \neq Y$).[45–47] However, up to now, it is still unclear how these specific Janus structures will affect their phonon transport behavior.

Motivated by the above statement, taking the Janus Pb$_2X$As (X = P, Sb, and Bi) monolayers as examples, we systematically investigate the thermal transport properties by means of first-principles calculations combined with Boltzmann transport theory. The calculations show that Pb$_2$PAs and Pb$_2$SbAs monolayers possess low lattice thermal conductivity. By the bonding and lattice dynamics analysis, we find that the strong phonon anharmonicity and the weak bond strength are the underlying mechanisms resulting in low κ_L in Pb$_2$PAs and Pb$_2$SbAs monolayers. The rest of the paper is organized as follows. In the next section, we give computational details about the phonon transport calculations. The third section shows the phonon transport properties of Pb$_2$PAs and Pb$_2$SbAs monolayers and the underlying physical mechanisms. Finally, we give the conclusion in the fourth section.

2. Computational details

In this work, the first-principles calculations are implemented in the Vienna *ab initio* simulation package (VASP).[48] The Perdew–Burke–Ernzerhof (PBE) generalized function of generalized gradient approximation (GGA) is used as the exchange correlation potential.[49] The wave functions are expanded in plane wave basis with the kinetic energy cutoff of 520 eV, and the k-mesh of $15 \times 15 \times 1$ is used to sample the Brillouin zone (BZ), with the energy convergence threshold setting as 10^{-9} eV. A large vacuum region is set as 15 Å to avoid the interactions between the monolayer and its mirrors induced by the periodic boundary conditions. The lattice constants and coordinates of all atoms are fully optimized until the maximum residual stress is less than 10^{-5} eV/Å. The harmonic approximation (HA) second-order interatomic force constants (2nd IFCs) and phonon dispersion are obtained by the ALAMODE package[50,51] via utilizing a finite displacement approach (0.02 Å) with a supercell of $5 \times 5 \times 1$, where the k-mesh is changed to $2 \times 2 \times 1$. It is worth noting that considering the special quadratic dispersion phenomenon present in the out-of-plane (ZA) mode of 2D materials, the 2nd IFCs in this paper are imposed with rotational sum rules.[52] Compressive sensing lattice dynamics (CSLD),[53–55] a method for achieving accelerated and accurate capture of higher-order IFCs, is used to obtain third-order anharmonic IFCs (3rd IFCs). Specifically, we perform a 5000-step *ab initio* molecular dynamics (AIMD) simulation at 300 K with a $4 \times 4 \times 1$ supercell (single Γ-point is used to sample the BZ). The AIMD simulations are performed using 1-fs time step and NVT ensemble (vibrations in the out-of-plane direction are fixed). We then sample 100 snapshot structures by skipping the first 1000 steps in the trajectories, using a frequency of 40 steps. Subsequently, to reduce the correlation between these atomic structures, every atom of the 100 snapshots is displaced by 0.1 Å along a random direction. Finally, we perform accurate static density functional theory calculations using a $3 \times 3 \times 1$ k-mesh to obtain the corresponding displacement and force datasets, thereby further fitting by the least absolute shrinkage and selection operator (LASSO) technique to obtain the 3rd IFCs. Once we obtain the 2nd IFCs and 3rd IFCs, by utilizing the iterative solution method implemented in the ShengBTE software,[56] the lattice thermal conductivity (κ_L) and phonon mode level information could be calculated via solving the phonon Boltzmann transport equation

$$\kappa_{L\alpha} = \sum_{\lambda} C_{\lambda} v_{\lambda\alpha}^2 \tau_{\lambda\alpha}, \tag{1}$$

where λ is the phonon mode index containing both phonon branch and wave vector, C_λ represents the mode heat capacity, $v_{\lambda\alpha}$ and $\tau_{\lambda\alpha}$ are the phonon group velocity and phonon lifetime along α lattice direction, respectively. The convergence of the lattice thermal conductivity is rigorously tested and the results are provided in Fig. 1. Ultimately, the 9th nearest neighbor atoms are used as interaction cutoff radius of 3rd IFCs and $71 \times 71 \times 1$ N-grid is chosen to calculate the convergent phonon information for Pb$_2X$As monolayers. Meanwhile, the effective thickness of 9.50 (9.72) Å is used to correct the thermal conductivity of the Pb$_2$PAs (Pb$_2$SbAs) monolayer.

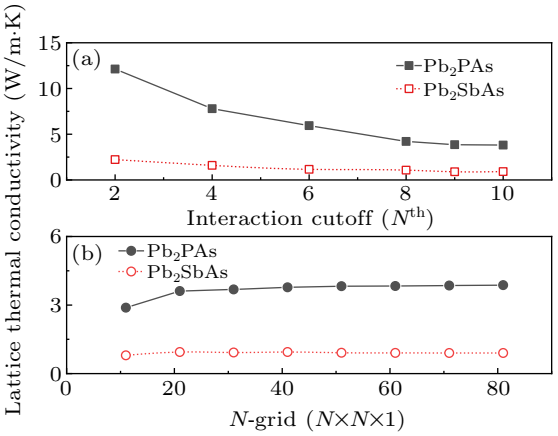


Fig. 1. (a) Third-order force constant interaction cutoff and (b) N-grid convergence tests for thermal conductivity of Pb$_2$PAs and Pb$_2$SbAs.

3. Results and discussion

As shown in the top view of Fig. 2(a), the Janus Pb$_2X$As (X = P, Sb, and Bi) monolayers exhibit a hexagonal honey-

comb structure similar to graphene. The difference in the outermost atoms results in the breaking of the mirror symmetry inherent in the D_{3h} symmetry group possessed by Pb_2X_2 (X = P, As, Sb, Bi), leading to the formation of the Janus structure with the C_{3v} symmetry group. The optimized structural parameters are listed in Table 1, where a and b represent lattice constants, L_1 represents X–Pb bond length, L_2 represents As–Pb bond length, L_3 represents Pb–Pb bond length, and AL represents the average bond length. Starting from the optimized geometry, the phonon spectrum of three Janus structures is obtained based on the finite displacement method. As shown in Figs. 1(b)–1(d), phonon dispersion curves with imaginary frequencies are absent in the Pb_2PAs and Pb_2SbAs monolayers. However, the Pb_2BiAs monolayer possesses very obvious imaginary frequencies, which implies that Pb_2BiAs is dynamically unstable. Therefore, the Pb_2BiAs is excluded from the subsequent discussion. The cutoff frequencies of the optical phonon modes of Pb_2PAs and Pb_2SbAs are significantly lower than those of graphene,[57,58] h-BN,[24,59] and other classical 2D materials.[60,61] Such behavior is usually due to weaker bonding.

Table 1. Calculated a and b for the lattice parameter of Janus Pb_2XAs monolayers.

	$a = b$ (Å)	L_1 (Å)	L_2 (Å)	L_3 (Å)	AL (Å)	AICOHP (eV)
Pb_2PAs	4.18	2.69	2.74	3.05	2.76	−3.39
Pb_2SbAs	4.39	2.92	2.81	3.05	2.90	−3.15
Pb_2BiAs	4.31	3.04	2.79	3.12	2.94	−2.79

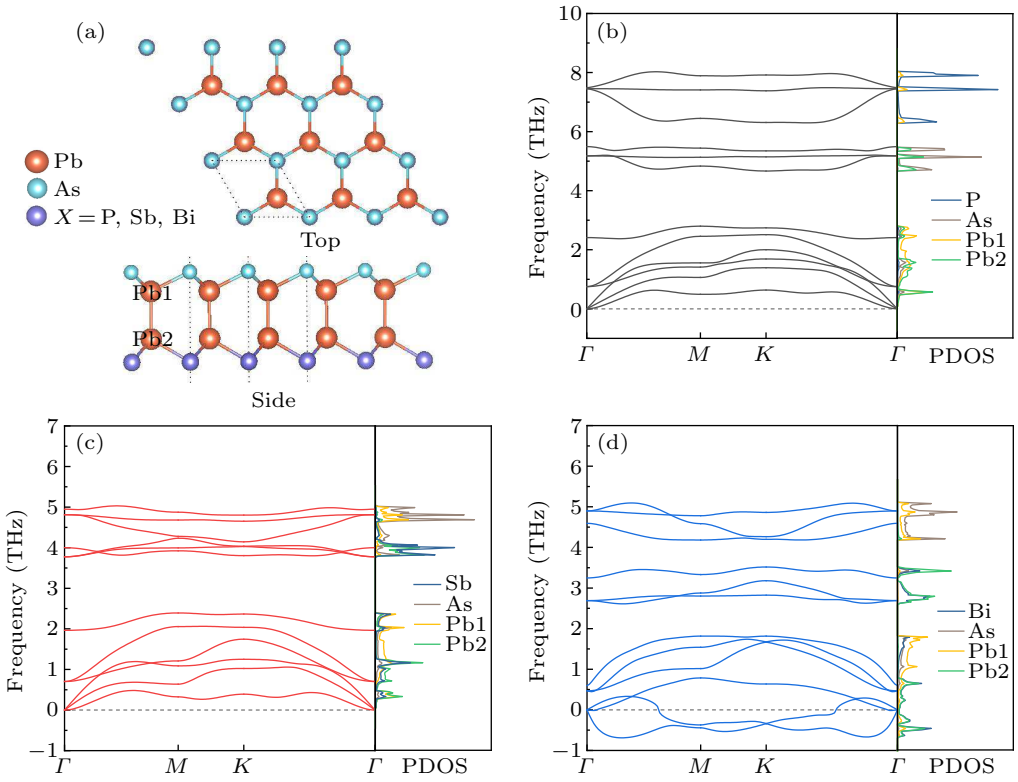


Fig. 2. (a) The top and side views of lattice structure of Janus Pb_2XAs (X = P, Sb, and Bi) monolayers. Phonon dispersion curves and projected density of states of (b) Pb_2PAs, (c) Pb_2SbAs, and (d) Pb_2BiAs.

In order to quantify the bonding strength of these materials, we calculate their integrated crystal orbital Hamilton population (ICOHP). Here, the ICOHP is calculated from the wave function file from VASP via using the LOBSTER package,[62] the strength of chemical bonds as a function of individual bonds can be easily quantified by the ICOHP values. In general, the smaller the absolute value of ICOHP, the weaker the chemical bond. As shown in Table 1, the average ICOHP (AICOHP) values of Pb_2PAs and Pb_2SbAs are −3.39 and −3.15, respectively, possessing significantly smaller negative values than those of graphene (−10.40)[58] and h-BN (−8.98).[59] Just as we analyzed above, the severely limited phonon vibrational frequencies in Pb_2PAs and Pb_2SbAs originate from weak bonding. Furthermore, to further understand the atomic contribution of the phonon branches, we plot the phonon projection density of states (PDOS) for each system. As shown in Fig. 2(b), one can find that the low-frequency phonon branch is mainly contributed by the heavy atom Pb in Pb_2PAs, while the high-frequency region is mainly contributed by the relatively light P and As atoms. Due to the large mass differences among all three Pb, P, and As atoms, two obvious phonon band gaps appear. In Pb_2SbAs, only one phonon band gap is observed and the band gap value decreases (see Fig. 2(c)). This phenomenon mainly stems from the presence of Sb atoms, which leads to the reduction of the mass difference between the atoms. Both in Pb_2PAs

and Pb_2SbAs, the acoustic and low-frequency optical phonons are entangled, leading to the absence of acoustic–optical band gap. The disappearance of acoustic–optical band gap suggests strong acoustic–optical coupling interactions, which could enhance the phonon–phonon scattering. Weak bonding as well as potentially strong phonon scattering often leads to a significant suppression of the thermal transport of the material, as can be insighted from many previous works.[59,63,64] Moreover, we calculated the electronic band structure of Pb_2PAs and Pb_2SbAs by using the HSE06 function.[65] Pb_2PAs and Pb_2SbAs both exhibit semiconducting characteristics, and the band gaps are 0.71 eV and 0.08 eV, respectively. Notably, the electronic properties of Pb_2PAs are studied in detail by Liu *et al*., calculating its band gap value as 0.72 eV.[45] Our results align with their study, confirming the reliability of our calculations.

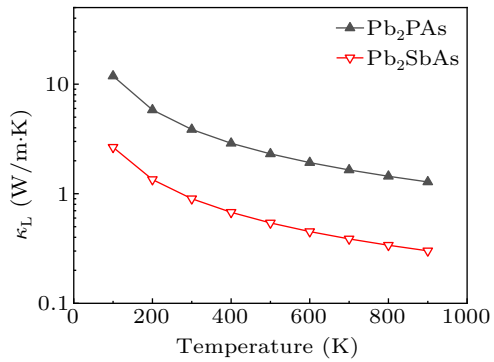


Fig. 3. Lattice thermal conductivity (κ_L) of Pb_2PAs and Pb_2AsSb at different temperatures.

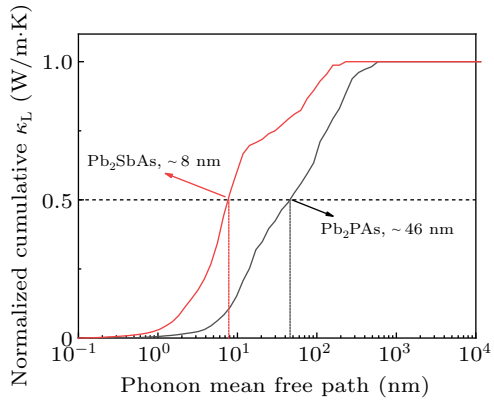


Fig. 4. Normalized cumulative lattice thermal conductivity (κ_L) at 300 K as a function of phonon mean free path (MFP) for Pb_2PAs and Pb_2AsSb.

In Fig. 3, we depict the lattice thermal conductivity (κ_L) of Pb_2PAs and Pb_2SbAs as a function of temperature. Both materials have poor thermal transport properties, and their thermal conductivity is at least two orders of magnitude lower than that of graphene and h-BN. The room temperature thermal conductivity of Pb_2SbAs (0.91 W/mK) is only a quarter of that of Pb_2PAs (3.88 W/mK). Moreover, the thermal conductivity decreases monotonically with temperature. This is a common phenomenon in most materials due to the enhancement of phonon–phonon scattering. We also further discuss the size effect on phonon transport in these two materials. The normalized cumulative κ_L values with respect to the phonon mean free path (MFP) are shown in Fig. 4. The size reduction can further reduce the sample thermal conductivity. When the size is reduced to 46 nm (8 nm), the thermal conductivity of Pb_2PAs (Pb_2SbAs) is reduced to half of the original. This provides some simple insights into the thermal transport of these materials on the micro-nano scale.

In order to reveal the origin of the low thermal conductivity of these Janus structures, phonon mode information including phonon group velocity (ν) and lifetime (τ) are systematically investigated. Since ν is proportional to $\sqrt{K/M}$, where K and M are respectively the bond strength and the atomic mass, low ν is also expected in materials with weak chemical bonds and large atomic masses. As shown in Fig. 5(a), both Pb_2PAs and Pb_2SbAs exhibit very low ν values (< 3 km/s), and the latter is overall lower than the former. Therefore, the low ν is one of the key factors contributing to the low lattice thermal conductivity of these two Janus materials. Phonon lifetime (τ) constitutes another pivotal factor that affects thermal conductivity. We further plot the τ of the two materials in Fig. 5(b), which is derived from the reciprocal of the phonon scattering rate. Evidently, both Pb_2SbAs and Pb_2PAs exhibit short τ, which implies strong anharmonic scattering. Moreover, Pb_2SbAs possesses shorter τ than that of Pb_2PAs, consistent with its exhibited thermal transport behavior. Consequently, the low lattice thermal conductivity of Pb_2PAs and Pb_2SbAs originates from the synergistic effect of low group velocity and short phonon lifetime.

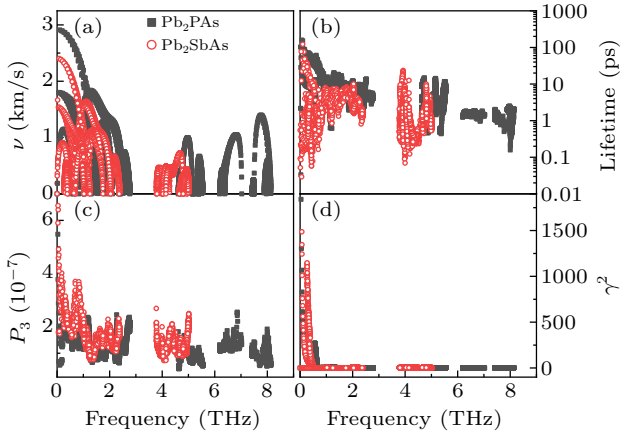


Fig. 5. Modal comparison of (a) group velocity (ν), (b) phonon lifetime (τ), (c) three-phonon scattering phase space (P_3), and (d) squared Grüneisen parameter (γ^2) for Pb_2PAs and Pb_2AsSb.

It is well known that scattering phase space (scattering probability) and phonon anharmonicity (scattering intensity) are the primary underlying mechanisms affecting phonon lifetime. Larger scattering phase space and anharmonicity lead to smaller phonon lifetime. Combining Figs. 5(c) and 5(d), one can find that the three-phonon scattering phase space (P_3) of Pb_2SbAs is only slightly larger than the P_3 of Pb_2PAs, but

the squared Grüneisen parameter (γ^2; quantifying the magnitude of phonon anharmonicity) of Pb_2SbAs is much larger than that of Pb_2PSb. Consequently, the major reason for the smaller phonon lifetime of Pb_2SbAs compared to Pb_2PAs is its stronger phonon anharmonicity. To further demonstrate the reliability of our results, we calculate the potential energy changes of the non-equivalent atoms of Pb_2PAs and Pb_2SbAs when they vibrate in different directions. As can be seen from Figs. 6(a) and 6(b), the fitted potential energy curves of each atom exhibit pronounced asymmetry when they make small vibrations along the direction of bond formation and out-of-plane direction based on the equilibrium position. This phenomenon implies that the system has strong anharmonicity, the magnitude of which can be reflected by the third-order term coefficients C. In Fig. 6(c), the absolute values of the fitted normalized anharmonic parameters ($|C|$) are compared for the non-equivalent atoms of Pb_2PAs and Pb_2SbAs. It is clear that the $|C|$ value of Sb_bf (Sb atoms vibrating along the direction of bond formation) is not significantly different from that of P_bf, but the $|C|$ value of Sb_out (Sb atoms vibrating in the out-of-plane direction) is significantly larger than those of P_out when Sb atoms are substituted for P atoms in Pb_2PAs. The stronger phonon anharmonicity in Pb_2SbAs is further demonstrated. In other words, the low lattice thermal conductivity of Pb_2PAs and Pb_2SbAs originates from the synergistic effect of strong phonon anharmonicity and low group velocity.

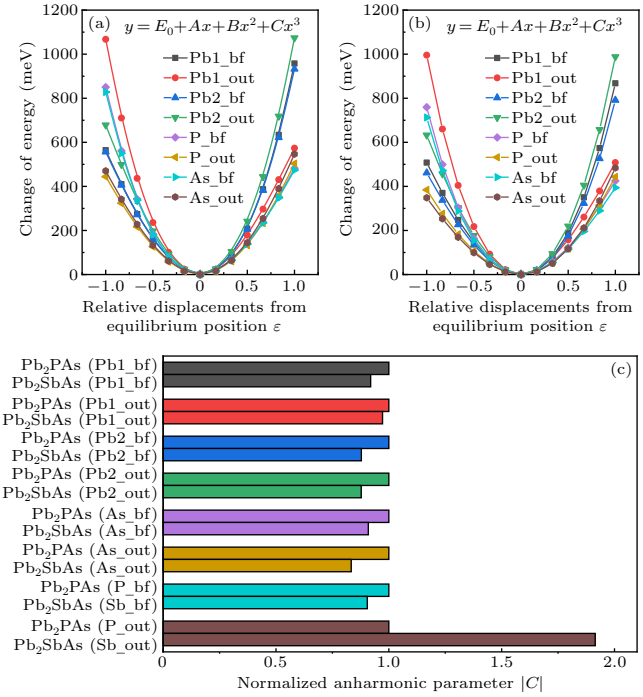


Fig. 6. Potential energy change of non-equivalent atoms for (a) Pb_2PAs and (b) Pb_2SbAs in different directions. (c) Comparison of fitted normalized anharmonic parameters ($|C|$) of non-equivalent atoms for Pb_2PAs and Pb_2SbAs.

The above discussion about anharmonicity only considers the three-phonon scattering process as such, while the more complex four-phonon scattering is not considered. This is mainly due to the fact that four-phonon scattering is often negligible compared to three-phonon scattering for most materials. Moreover, the computation of the Boltzmann transport equation containing four-phonon scattering using first-principles is quite time-consuming. To avoid huge computational costs, the relative regular residuals (RRR) are used in this paper to investigate the anharmonic effects of different atomic vibrations.[13,59,66,67] When the four-phonon anharmonicity is small enough, the RRR exhibits the shape of "$\sim$" or "$\backsim$". Otherwise, it has a "W" or "M" shape. As shown in Fig. S1 , we plot the relative regular residuals of nonequivalent atoms for Pb_2PAs and Pb_2SbAs along different directions. Apparently, four-phonon scattering is not dominant in Pb_2PAs and Pb_2SbAs. Therefore, we speculate that the thermal transport in these systems may be only slightly suppressed after considering four-phonon. That is to say, the four-phonon processes are limited in Pb_2PAs and Pb_2SbAs, and the three-phonon scattering is sufficient to describe their anharmonicity.

4. Conclusion

We have systematically investigated the thermal transport properties of Janus Pb_2PAs and Pb_2SbAs monolayers by using the first-principles calculations combined with the Boltzmann transport equation. Both materials have poor thermal transport properties, and their thermal conductivity is at least two orders of magnitude lower than that of graphene and h-BN. The room temperature thermal conductivity of Pb_2SbAs (0.91 W/mK) is only a quarter of that of Pb_2PAs (3.88 W/mK). Further studies reveal that the synergistic effect of low group velocity due to weak bonding and strong phonon anharmonicity is the fundamental cause of the intrinsic low thermal conductivity in these Janus structures. Furthermore, in order to reveal the underlying mechanism of the phenomenon that the thermal conductivity of Pb_2SbAs is much smaller than that of Pb_2PAs, we compare the scattering phase space and Grüneisen parameter of these materials. It is found that phonon anharmonicity, as reflected by the Grüneisen parameter, is the main factor causing this phenomenon. We obtain energy versus displacement curves based on varying the atomic displacements and quantify the deviations from the harmonic approximation, further confirming the anharmonic variation of Pb_2PAs and Pb_2SbAs. Relative regular residual analysis further indicates that the four-phonon processes are limited in Pb_2PAs and Pb_2SbAs, and the three-phonon scattering is sufficient to describe their anharmonicity. The finding presented in this work could shed light on the thermal transport properties of Janus Pb_2PAs and Pb_2SbAs monolayers, and the low lattice thermal conductivity endows the potential applications in the field of thermal barriers and thermoelectrics.

Acknowledgments

Project supported by the Youth Science and Technology Talent Project of Hunan Province of China (Grant No. 2022RC1197) and the National Natural Science Foundation of China (Grant No. 52372260).

References

[1] Liu B, Liu Y, Zhu C, Xiang H, Chen H, Sun L, Gao Y and Zhou Y 2019 *J. Mater. Sci. Technol.* **35** 833
[2] Padture N P, Gell M and Jordan E H 2002 *Science* **296** 280
[3] Bell L E 2008 *Science* **321** 1457
[4] Qin B, Wang D, Liu X, Qin Y, Dong J F, Luo J, Li J W, Liu W, Tan G, Tang X, Li J F, He J and Zhao L D 2021 *Science* **373** 556
[5] Snyder G J and Toberer E S 2008 *Nat. Mater.* **7** 105
[6] Ouyang T, Jiang E, Tang C, Li J, He C and Zhong J 2018 *J. Mater. Chem. A* **6** 21532
[7] Ouyang T and Hu M 2015 *Phys. Rev. B* **92** 235204
[8] Wei D, Zhou E, Zheng X, Wang H, Shen C, Zhang H, Qin Z and Qin G 2022 *NPJ Comput. Mater.* **8** 260
[9] Shahsavar A, Salimpour M R, Saghafian M and Shafii M B 2016 *J. Mech. Sci. Technol.* **30** 809
[10] Ouyang T, Liu Q, Chen M, Tang C, Li J, Zhang C, He C, Bao H, Zhong J and Hu M 2019 *ES Energy Environ.* **3** 88
[11] Tian Z, Garg J, Esfarjani K, Shiga T, Shiomi J and Chen G 2012 *Phys. Rev. B* **85** 184303
[12] Hu M and Poulikakos D 2012 *Nano Lett.* **12** 5487
[13] Tang Z, Wang X, Li J, He C, Chen M, Tang C and Ouyang T 2023 *Phys. Rev. B* **108** 214304
[14] Skoug E J and Morelli D T 2011 *Phys. Rev. Lett.* **107** 235901
[15] Schweika W, Hermann R P, Prager M, Perßon J and Keppens V 2007 *Phys. Rev. Lett.* **99** 125501
[16] Paschen S, Carrillo-Cabrera W, Bentien A, Tran V H, Baenitz M, Grin Y and Steglich F 2001 *Phys. Rev. B* **64** 214404
[17] Lee S, Esfarjani K, Luo T, Zhou J, Tian Z and Chen G 2014 *Nat. Commun.* **5** 3525
[18] Peng B, Zhang H, Shao H, Xu Y, Ni G, Zhang R and Zhu H 2016 *Phys. Rev. B* **94** 245420
[19] Gu X, Wei Y, Yin X, Li B and Yang R 2018 *Rev. Mod. Phys.* **90** 041002
[20] Seol J H, Jo I, Moore A L, Lindsay L, Aitken Z H, Pettes M T, Li X, Yao Z, Huang R, Broido D, Mingo N, Ruoff R S and Shi L 2010 *Science* **328** 213
[21] Balandin A A 2011 *Nat. Mater.* **10** 569
[22] Feng T, Lindsay L and Ruan X 2017 *Phys. Rev. B* **96** 161201
[23] Sadeghi M M, Pettes M T and Shi L 2012 *Solid State Commun.* **152** 1321
[24] Fan H, Wu H, Lindsay L and Hu Y 2019 *Phys. Rev. B* **100** 085420
[25] Cai Q, Scullion D, Gan W, Falin A, Zhang S, Watanabe K, Taniguchi T, Chen Y, Santos E J G and Li L H 2019 *Sci. Adv.* **5** eaav0129
[26] Li W, Carrete J and Mingo N 2013 *Appl. Phys. Lett.* **103** 253103
[27] Liu X, Zhang G, Pei Q X and Zhang Y W 2013 *Appl. Phys. Lett.* **103** 133113
[28] Jiang J W, Park H S and Rabczuk T 2013 *J. Appl. Phys.* **114** 064307
[29] Ashton M, Sinnott S B and Hennig R G 2016 *Appl. Phys. Lett.* **109** 192103
[30] Özdamar B, Özbal G, Çınar M N, Sevim K, Kurt G, Kaya B and Sevinçli H 2018 *Phys. Rev. B* **98** 045431
[31] Li L, Wang W, Gong P, Zhu X, Deng B, Shi X, Gao G, Li H and Zhai T 2018 *Adv. Mater.* **30** 1706771
[32] Barreteau C, Michon B, Besnard C and Giannini E 2016 *J. Cryst. Growth* **443** 75
[33] Kim D, Park K, Lee J H, Kwon I S, Kwak I H and Park J 2021 *Small* **17** 2006310
[34] Lee K, Kamali S, Ericsson T, Bellard M and Kovnir K 2016 *Chem. Mater.* **28** 2776
[35] Cheng A Q, He Z, Zhao J, Zeng H and Chen R S 2018 *ACS Appl. Mater. Interfaces* **10** 5133
[36] Chen Q Y, Huang F J, Ruan J Q, Ma T, Xiong K and He Y 2022 *Phys. Rev. Mater.* **6** 104005
[37] Ozbey D H, Kilic M E and Durgun E 2022 *Phys. Rev. Appl.* **17** 034043
[38] Huang B, Zhuang H L, Yoon M, Sumpter B G and Wei S H 2015 *Phys. Rev. B* **91** 121401
[39] Somaiya R N, Sonvane Y A and Gupta S K 2020 *Phys. Chem. Chem. Phys.* **22** 3990
[40] Niasadegh N, Naseri M and Rezaee S 2021 *Opt. Quantum Electron.* **53** 502
[41] Huang H H, Fan X, Singh D J and Zheng W T 2019 *J. Mater. Chem. C* **7** 10652
[42] Wu Y, Yang C H, Zhang H N, Zhu L H, Wang X Y, Li Y Q, Zhu S Y and Wang X C 2022 *Appl. Surf. Sci.* **589** 152999
[43] He Q W, Wu Y, Yang C H, Zhang H N, Tang D S, Shang X and Wang X C 2023 *Nanoscale* **15** 10458
[44] Liu H Y, Wang Y Y, Chen Z Y, Hou T P, Wu K M and Lin H F 2023 *Phys. Chem. Chem. Phys.* **25** 16559
[45] Liu M Y, Gong L, He Y and Cao C 2021 *Phys. Rev. B* **104** 035409
[46] Liu M Y, Gong L, He Y and Cao C 2021 *Phys. Rev. B* **103** 075421
[47] Babaee Touski S and Ghobadi N 2021 *Phys. Rev. B* **103** 165404
[48] Kresse G and Furthmuller J 1996 *Phys. Rev. B* **54** 11169
[49] Perdew J P, Burke K and Ernzerhof M 1996 *Phys. Rev. Lett.* **77** 3865
[50] Tadano T and Tsuneyuki S 2015 *Phys. Rev. B* **92** 054301
[51] Tadano T, Gohda Y and Tsuneyuki S 2014 *J. Phys.: Condens. Matter* **26** 225402
[52] Taheri A, Pisana S and Singh C V 2021 *Phys. Rev. B* **103** 235426
[53] Zhou F, Nielson W, Xia Y and Ozoliņš V 2019 *Phys. Rev. B* **100** 184308
[54] Zhou F, Sadigh B, Åberg D, Xia Y and Ozoliņš V 2019 *Phys. Rev. B* **100** 184309
[55] Zhou F, Nielson W, Xia Y and Ozoliņš V 2014 *Phys. Rev. Lett.* **113** 185501
[56] Li W, Carrete J, Katcho N A and Mingo N 2014 *Comput. Phys. Commun.* **185** 1747
[57] Nika D L and Balandin A A 2017 *Rep. Prog. Phys.* **80** 036502
[58] Yu L, Chen A, Wang X, Wang H, Qin Z and Qin G 2022 *Phys. Rev. B* **106** 125410
[59] Tang Z, Wang X, Li J, He C, Chen M, Li X, Tang C and Ouyang T 2023 *Appl. Phys. Lett.* **123** 102201
[60] Xie H, Hu M and Bao H 2014 *Appl. Phys. Lett.* **104** 131906
[61] Wang X and Tabarraei A 2016 *Appl. Phys. Lett.* **108** 191905
[62] Maintz S, Deringer V L, Tchougréeff A L and Dronskowski R 2016 *J. Comput. Chem.* **37** 1030
[63] Feng Z, Fu Y, Zhang Y and Singh D J 2020 *Phys. Rev. B* **101** 064301
[64] Mukhopadhyay S, Singh D J and Reinecke T L 2020 *Chem. Mater.* **32** 8906
[65] Heyd J, Scuseria G E and Ernzerhof M 2003 *J. Chem. Phys.* **118** 8207
[66] Yue S Y, Qin G, Zhang X, Sheng X, Su G and Hu M 2017 *Phys. Rev. B* **95** 085207
[67] Yue S Y, Zhang X, Qin G, Phillpot S R and Hu M 2017 *Phys. Rev. B* **95** 195203